MOLECULAR AND CELLULAR BIOLOGY, May 2005, p. 4129–4137 Vol. 25, No. 10
0270-7306/05/$08.00+0 doi:10.1128/MCB.25.10.4129–4137.2005

The Ciliary Rootlet Maintains Long-Term Stability of Sensory Cilia

Jun Yang,[1]* Jiangang Gao,[2] Michael Adamian,[1] Xiao-Hong Wen,[3] Basil Pawlyk,[1] Luo Zhang,[4]† Michael J. Sanderson,[4] Jian Zuo,[2] Clint L. Makino,[3] and Tiansen Li[1]*

The Berman-Gund Laboratory for the Study of Retinal Degenerations[1] and Howe Laboratory,[3] Department of Ophthalmology, Harvard Medical School, Massachusetts Eye and Ear Infirmary, Boston, Massachusetts 02114; Department of Developmental Neurobiology, St. Jude Children's Research Hospital, Memphis, Tennessee[2]; and Department of Physiology, University of Massachusetts Medical School, Worcester, Massachusetts[4]

Received 19 November 2004/Returned for modification 2 December 2004/Accepted 25 February 2005

The striated ciliary rootlet is a prominent cytoskeleton originating from basal bodies of ciliated cells. Although a familiar structure in cell biology, its function has remained unresolved. In this study, we carried out targeted disruption in mice of the gene for rootletin, a component of the rootlet. In the mutant, ciliated cells are devoid of rootlets. Phototransduction and ciliary beating in sensory and motile cilia initially exhibit no apparent functional deficits. However, photoreceptors degenerate over time, and mutant lungs appear prone to pathological changes consistent with insufficient mucociliary clearance. Further analyses revealed a striking fragility at the ciliary base in photoreceptors lacking rootlets. In vitro assays suggest that the rootlet is among the least dynamic of all cytoskeletons and interacts with actin filaments. Thus, a primary function of the rootlet is to provide structural support for the cilium. Inasmuch as photoreceptors elaborate an exceptionally enlarged sensory cilium, they are especially dependent on the rootlet for structural integrity and long-term survival.

The ciliary rootlet originates from the proximal ends of basal bodies, the centriole-related structure that anchors the cilia, and extends proximally toward the cell nuclei (5, 25). Prominent rootlets are associated with sensory cilia of photoreceptor cells and motile cilia, such as those lining the respiratory tract, oviduct, and brain ventricles. The retinal photoreceptor elaborates a single enlarged distal cilium known as the outer segment. The outer segment is packed with photosensitive membranous disks and specializes in phototransduction. It is among the largest of all mammalian cilia, spanning approximately 25 μm in length and more than 1 μm in diameter. The outer segment is linked to the cell body, the inner segment, through a thin bridge called the connecting cilium (3). In a photoreceptor, the rootlet appears as a very thick striated filament that traverses the entire cell body all the way to the synaptic terminal (17, 19, 26). In epithelial cells bearing motile cilia, rootlets appear as robust subapical filamentous networks.

A number of hypothetical functions have been ascribed to the rootlets. Their cytoskeletal appearance suggests a role as a critical support structure for the cilia, especially in situations where mechanical stress is expected to be high. For example, the junction where the photoreceptor connecting cilium meets the inner segment may be particularly dependent on the rootlet for support against shear forces incurred during eye movements or trauma. Although motile cilia are tiny in comparison, they may also be subjected to mechanical strain imposed by vigorous ciliary beating. An additional role in the proper positioning or anchoring of cellular organelles is implicated by the association of photoreceptor rootlets with membrane-bound saccules, endoplasmic reticulum (ER), Golgi membranes, and mitochondria (19, 24). Finally, a role for rootlets in intracellular protein transport has also been suggested (4). Provision of structural support, organization of cellular organelles and participation in intracellular trafficking seem plausible hypotheses, but none was tested directly.

It was recently shown that rootletin, a large protein composed almost entirely of coiled-coil domains, is a structural component of the ciliary rootlet (26). It was suggested that the ciliary rootlets are composed of polymerized rootletin fibers bundled into thick filaments (26). In this study, we carried out targeted disruption of the rootletin gene and confirmed that rootletin is the major structural constituent of the ciliary rootlet. Our in vivo and in vitro analyses define the functions of the ciliary rootlet.

MATERIALS AND METHODS

Generation of rootletin mutant mouse. An 8-kb rootletin genomic fragment containing exons 2 to 8 was amplified from 129/Sv mouse DNA by PCR. After several steps of cloning, the 1.4-kb BamHI/EcoRI fragment and the 4.9-kb EcoRI/DraI fragment of the resulting PCR product were inserted separately as the short arm and long arm, respectively, into a modified pGT-N29 vector, which contained a diphtheria toxin expression cassette as a negative selection marker (Fig. 1A). The targeting vector was linearized and electroporated into R1 embryonic stem (ES) cells. Three ES clones were found to have the Neo^r gene and additional intronic sequences inserted into intron 3 of the rootletin gene. Two clones, 1H3 and 1H6, were microinjected into C57BL/6 blastocysts. The resulting chimeras were crossed with C57BL/6 mice. Heterozygous and homozygous mice were identified with respect to the targeted allele by PCR. The two mutant lines had the same degree of disruption in mRNA and protein expression as shown by reverse transcription-PCR (RT-PCR) and Western blotting. We therefore focused our studies on the 1H3 line. All procedures on animals followed institutional guidelines. Littermate wild-type (WT) and, in many instances, littermate heterozygote (+/–) mice were used as normal controls, as the latter had levels of rootletin comparable to those of WT and normal-appearing rootlets (see Results).

Antibodies, Western blotting, immunofluorescence, and electron microscopy. Rootletin, RPGR, rhodopsin, and cone opsin antibodies were described previously (9, 14, 26). Monoclonal anti-acetylated α-tubulin and antiactin antibodies were obtained from Sigma-Aldrich. Monoclonal antitubulin (DM1A and DM1B)

* Corresponding author. Mailing address: Massachusetts Eye and Ear Infirmary, 243 Charles St., Boston, MA 02114. Phone: (617) 573-3904. Fax: (617) 753-3216. E-mail: tli@meei.harvard.edu.

† Present address: Department of Otolaryngology, Head and Neck Surgery, Capital University of Medical Sciences, Beijing Tong Ren Hospital, Beijing, People's Republic of China.

antibodies were from Abcam Limited. Immunoprecipitation, Western blotting, immunofluorescence, and electron microscopy were performed as described previously (26). To test for protein translocation between the photoreceptor inner and outer segments, mice were adapted to the dark overnight. They were anesthetized, and their pupils were dilated and exposed to bright light for 15 min before being processed for immunofluorescence.

Cell culture, transient transfection, time-lapse video, and FRAP. COS-7 cells were cultured and transiently transfected as previously described (26). Mouse full-length rootletin or vimentin cDNA was expressed in the pEGFP-C2 vector. For live-cell imaging, cells were grown on plastic plates in complete normal growth medium with 25 mM HEPES. A heating plate (model 2412ps-12W-B30; Brook Industries) was placed on the stage of the microscope to maintain the temperature of the cells at about 32°C. Time-lapse video and fluorescence recovery after photobleaching (FRAP) were performed with a confocal laser scanning microscope (model TCS SP2; Leica) using Leica confocal software. The bleached regions of the cells were defined manually as about 1.5-μm-wide bars with a 1.2-μm depth at the *z* axis. To bleach the fluorescence, three z-plates were bleached one by one for a total of 5 min using 100% laser power. The post-bleaching images were taken at 10-min intervals for a total of 110 min. The intensities of the photobleached regions were measured and normalized to the intensities of the same region before photobleaching (photobleaching effect) and the neighboring regions at the same time point (autobleaching effect during the recording). Control experiments were conducted using formaldehyde-fixed vimentin-transfected cells. Rootletin staining of cells immediately fixed after a 15-min bleaching demonstrated no damage to the integrity of rootletin fibers from the bleaching (data not shown). Fast-stage fluorescence recovery usually occurs within minutes after photobleaching (1, 16, 21). It may happen on the two unbleached z-plates at the time when the laser beam bleaches the third z-plate. Therefore, our FRAP protocol did not record fluorescence recovery at the fast stage.

Measurement of the outer segment length and the number of the dissociated outer segments. To measure the lengths of photoreceptor outer segments, we used two methods. First, dissected retina was chopped finely in phosphate-buffered saline and spread on polylysine-coated glass slides. Pictures were taken at random views through a 40× objective on a microscope (model IX70; Olympus) using a digital camera (Carl Zeiss MicroImaging, Inc.). The length of the dissociated outer segments was measured using Adobe Photoshop software. To ensure that the dissociated outer segments were full length, only the ones with connecting cilia attached were measured. Second, the dissected retina was fixed overnight. The thickness of the outer-segment layer on the sectioned retina was measured as the length of the outer segments under the microscope.

To compare the numbers of dissociated outer segments between the control and mutant groups, gently dissected retina was gently sucked twice using a smooth-opening glass pipette in 200 μl of BGJb medium (Gibco). The number of dissociated photoreceptors in the medium was counted using a hemocytometer (Reichert).

ERG and single-cell suction electrode recording. Electroretinogram (ERG) recording was performed as described previously (12). Four mutant and three littermate control mice were used for single-cell suction electrode recording as described previously (13).

Measurement of ciliary-beating frequency. Primary cultures of mouse tracheal epithelial cells and measurement of ciliary-beating frequency were performed as previously described (29) with the following changes. Two-month-old mice were sacrificed by intraperitoneal injection of Nembutal (12 ml/kg of body weight). The trachea was removed between the larynx and the collarbone. In Dulbecco's modified Eagle's medium supplemented with 10% fetal bovine serum and penicillin-streptomycin, the trachea was cut into three pieces by severing between the cartilaginous rings. Each piece was cut into two parts parallel to the length of the trachea. With the curved mucous membrane facing up, the tissue was sliced into strips with longitudinal rolling cuts across the cartilage rings. The final trachea strips were placed onto rat tail collagen-coated glass coverslips and cultured in Dulbecco's modified Eagle's medium with 10% CO_2 at 37°C for 3 to 5 days.

Analysis of lung pathology. Lungs were first fixed in methanol-acetone-acetic acid (50:50:5) for about 1 h and then switched to 4% formaldehyde–phosphate-buffered saline. Fixed lungs were embedded in paraffin, sectioned, and stained with hematoxylin and eosin. Under the microscope, lymphocyte infiltration was analyzed according to the following standards: −, no lymphocyte infiltration was observed; +, lymphocyte infiltration was observed in several small regions; ++, lymphocyte infiltration was found in many small regions; and +++, lymphocytes infiltrated almost everywhere on the lung section. Charcot-Leyden crystals in humans are enriched for galectin-10, but in mice similar crystals are highly enriched for the protein Ym1 (7). Therefore, immunofluorescence with a Ym1 antibody (22) was done on paraffin sections of the lungs.

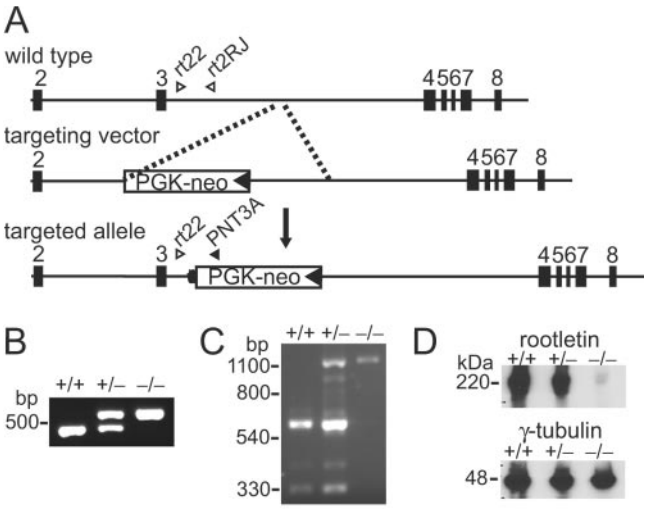

FIG. 1. Generation of the rootletin mutant. (A) Targeting strategy for disrupting the rootletin gene. PCR primers for the identification of the mutant and WT alleles are shown as arrowheads. (B) Identification of the mutant allele by genomic PCR. (C) Analysis of the rootletin transcript by RT-PCR shows the loss of the normal transcript (at 607 bp) and the appearance of an aberrant transcript (at 1,105 bp) in the homozygous mutant. (D). The rootletin protein essentially disappears in the homozygous mutant as shown on an immunoblot. The rootletin level was minimally reduced in the heterozygotes. γ-Tubulin is shown as a loading control. +/+, WT; –/–, homozygous mutant; +/–, heterozygotes.

Statistical analysis. Persons performing quantitative measurements in most instances were unaware of the genotypes. The Student *t* test was conducted to compare the measured values for control and mutant mice. A *P* value of less than 0.05 was considered to indicate a significant difference between the two groups.

RESULTS

Loss of rootletin abolishes the formation of the ciliary rootlet. The targeted allele carried an insertion of the Neo^r expression cassette and additional sequences in the rootletin gene (Fig. 1A) (see Materials and Methods). Genotyping by PCR (Fig. 1B) found offspring of different genotypes at the expected Mendelian ratios, indicating that homozygotes were viable. Homozygotes appeared comparable to WT littermates in reproductive performance and general health. To determine whether the targeted allele had been insertionally inactivated, we analyzed rootletin expression in the retina, where its level is normally the highest (26). RT-PCR using a primer pair spanning exons 3 through 7 detected no normal transcript in the homozygotes; instead an aberrant, larger PCR product was seen (Fig. 1C). By sequencing, this was found to result from a 498-bp insertion of the Neo^r C-terminal sequence, indicating aberrant RNA splicing. Although the insertion did not result in a frameshift, there was nevertheless little accumulation of a protein product from the mutant transcript. As shown in Fig. 1D, immunoblotting detected only a trace amount of rootletin-related polypeptide in the homozygotes, even after the blots were overdeveloped. Thus, the targeted rootletin allele was close to being a null allele.

To see whether the ciliary rootlet was ablated upon loss of rootletin, immunofluorescence was performed on sections of

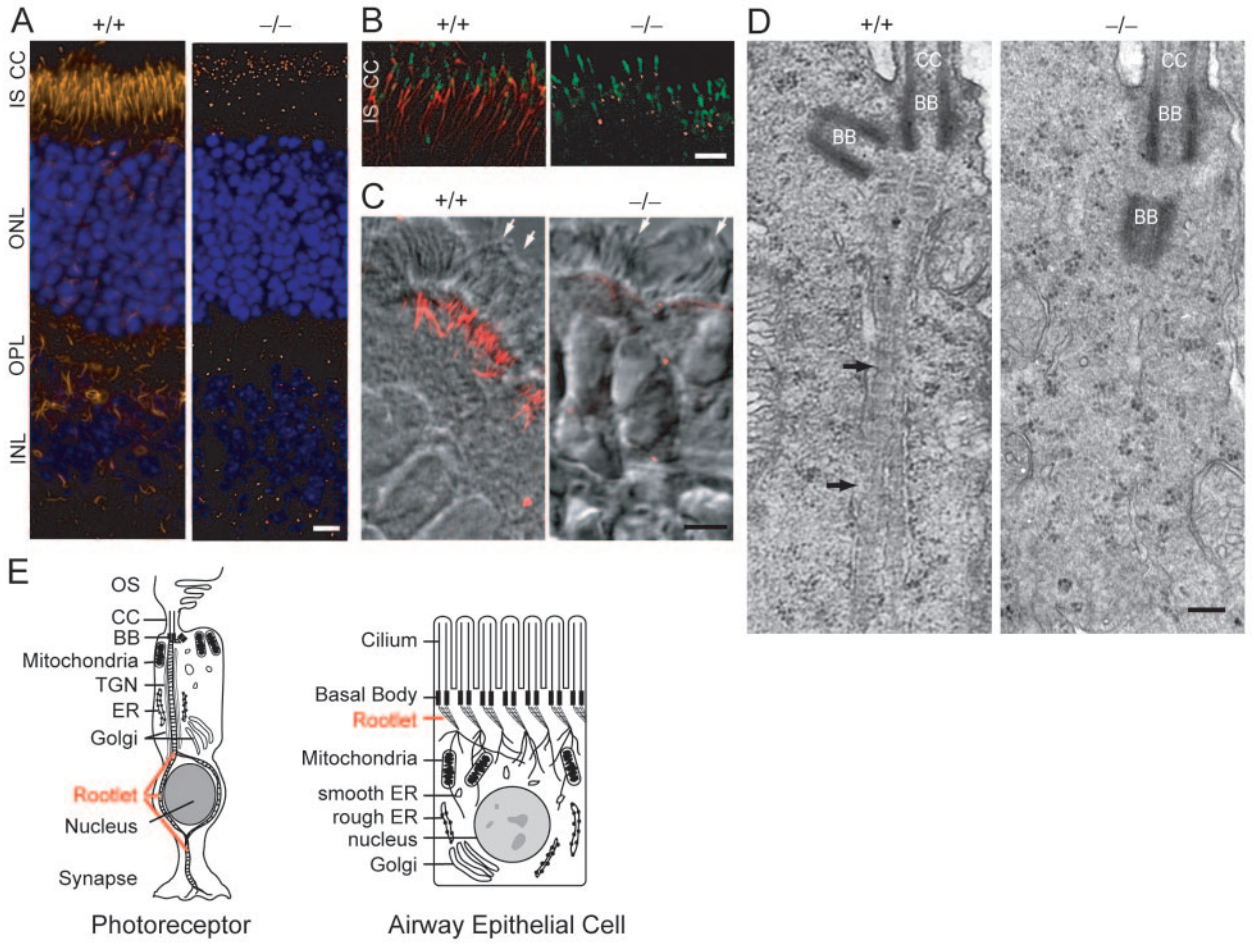

FIG. 2. Absence of ciliary rootlets in photoreceptors (A, B, and D) and in airway epithelia (C) of the homozygous mutant. (A) By immunofluorescence, rootlets (red) are seen traversing the inner segments and to a lesser extent through the outer nuclear layer. These are absent in the mutant. Cell nuclei (blue) were counterstained with Hoechst dye 33342. (B) Double labeling for RPGR (green; a connecting cilium marker) and rootlets (red) shows rootlets extending proximally from the cilia in a WT mouse but appearing only as tiny speckles in the mutant. Note the gaps between the cilium and rootletin staining where basal bodies are located. (C) Rootlets (red) are absent in the airway epithelia of the mutant. Immunofluorescence and Nomarski images are superimposed. White arrows indicate the tips of motile cilia. (D) Loss of the rootlet revealed by electron microscopy. In the WT (+/+) photoreceptor, a striated rootlet (arrows) originates from the basal bodies (BB) below the connecting cilium (CC) and extends proximally. There is no rootlet in the mutant (–/–). The basal bodies are typically arranged at a right angle in the WT but appear more longitudinally aligned in the mutant, where the rootlet is absent. (E) Schematic representations of a photoreceptor and an airway epithelial cell. OS, outer segment; IS, inner segment; INL, inner nuclear layer; ONL, outer (photoreceptor) nuclear layer; TGN, trans-Golgi network. Bars, 10 μm in panels A and B, 5 μm in panel C, and 0.2 μm in panel D.

retina and trachea. In the mutant retina, only rabbit Root6 antibody with the highest sensitivity, but not other rootletin antibodies, detected a weak rootletin signal (Fig. 2). In contrast to WT photoreceptors, where rootletin stained as prominent filaments, the mutant had tiny speckles (Fig. 2A and B), restricted to what appeared to be the proximal ends of basal bodies (Fig. 2B). Similarly, in airway epithelia strong immunofluorescence for rootletin fibers was seen in the WT, but only traces of staining were present in the mutant. The residual rootletin staining appeared just beneath the apical plate, juxtaposing to the row of basal bodies in these cells (Fig. 2C). Electron microscopy confirmed the absence of rootlets in the mutant, while robust striated rootlets were seen in the WT photoreceptors (Fig. 2D). Survey by rootletin immunofluorescence showed loss of rootletin fibers in multiple ciliated epithelia, where rootlets are normally found (data not shown). Together with previous findings that rootletin alone polymerizes into fibers resembling native rootlets in cell culture and that no other proteins of comparable abundance coimmunoprecipitated with rootletin (26), these data support the notion that the ciliary rootlet is composed of rootletin homopolymers. Thus, rootletin is likely the sole structural constituent of the rootlet.

The ciliary rootlet has no determinant roles in ciliary development and basal functions of the cilia. By light and electron microscopy, retinal photoreceptors and epithelia bearing motile cilia appeared normal morphologically in younger animals (under 3 months) (Fig. 2). ERGs, elicited by flashes of light, reflect signal transduction within rod and cone photoreceptors and excitation of the secondary retinal neurons. ERGs of both rods and cones were found to be normal in the younger mutant mice (data not shown). Single-photoreceptor record-

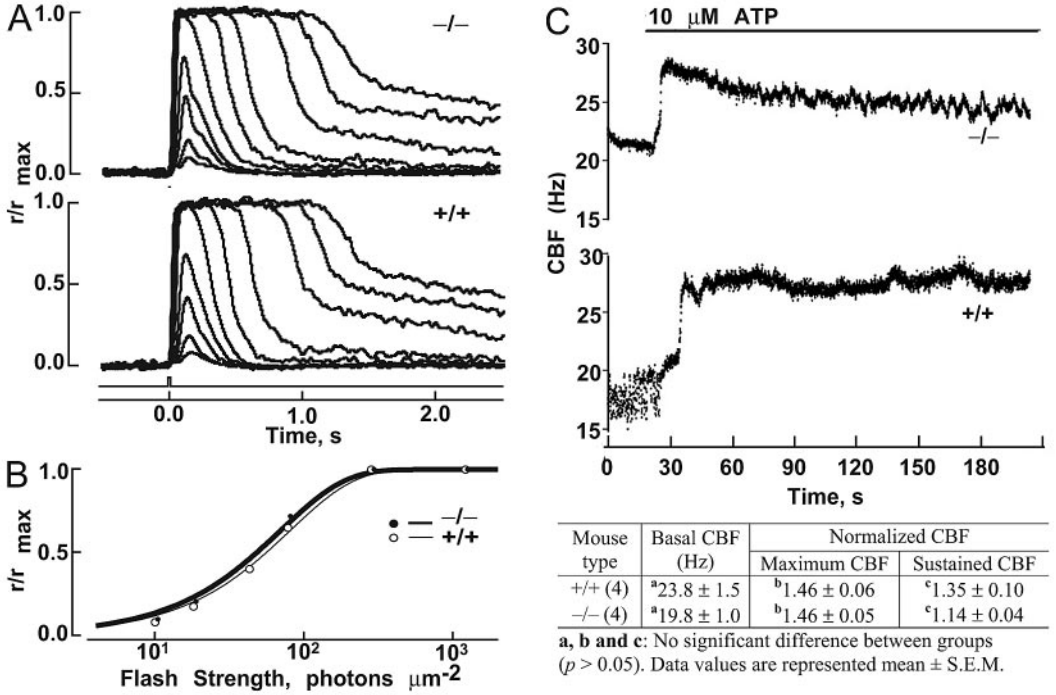

Mouse type	Basal CBF (Hz)	Normalized CBF	
		Maximum CBF	Sustained CBF
+/+ (4)	[a]23.8 ± 1.5	[b]1.46 ± 0.06	[c]1.35 ± 0.10
–/– (4)	[a]19.8 ± 1.0	[b]1.46 ± 0.05	[c]1.14 ± 0.04

a, b and c: No significant difference between groups ($p > 0.05$). Data values are represented mean ± S.E.M.

FIG. 3. Flash responses of single rods and measurements of ciliary beating frequency. (A) Averaged responses of the mutant (–/–) and WT (+/+) rods. The maximum amplitude was 11 pA for both rods. The flash monitor is shown below the responses. (B) Stimulus-response relations for the WT (○) and mutant (●) cells in panel A. Results were fit (continuous lines) as follows: $r/r_{max} = 1 - \exp(-ki)$, where r was response amplitude, i was flash strength, k was $\ln(2)/i_o$, and i_o was the flash strength producing a half-maximal response. (C) Ciliary beating is normal in the rootletin mutant mice. The upper panel shows recordings of a representative cilium from each group. The lower panel is a summary of basal ciliary beating frequency (CBF) and responses to ATP from the mutant and WT controls. Both basal levels of ciliary beating and responses to the addition of ATP are comparable between the mutant and the control. Normalized CBF, the ratio of CBF after the ATP addition to basal CBF; maximum CBF, maximum normalized CBF; sustained CBF, normalized CBF at 210 s.

ings, which provide greater detail for response characteristics of the rods, showed normal response kinetics (Fig. 3A; also see Table 1) and flash sensitivity (Fig. 3B). Thus, disruption of rootletin had no significant effect on phototransduction in rods. Notably, whereas those mutant photoreceptors that did respond to flash stimuli exhibited normal characteristics, a large percentage of them failed to respond at all. These "dead" cells were likely to have lost their membrane integrity attributable to the fragility of the mutant cells (see below for further discussion).

To examine whether the ciliary rootlet is fundamental to the movement of motile cilia, we analyzed the beating of tracheal cilia in mutant mice. Cilia in the mutants were motile and beat coordinately at a frequency similar to that of the WT (Fig. 3C).

TABLE 1. Flash response parameters of single rods[a]

Mice	i_o (photons · μm^{-2})	Time to peak (ms)	Integration time (ms)
Rootletin$^{-/-}$	47 ± 5 (13)	136 ± 6 (12)	262 ± 16 (12)
WT	54 ± 5 (16)	120 ± 4 (14)	284 ± 31 (12)

[a] Values are means ± SEM. Values in parentheses are numbers of rods. i_o is the flash strength at 500 nm producing a half-maximal response. Time to peak and integration time refer to dim-flash responses whose amplitudes were <0.2 r_{max}. The dim-flash response has the same kinetics as the single-photon response. Integration time is the response integral divided by response amplitude. P values (t test) were as follows: for i_o, 0.28; for time to peak, 0.04; and for integration time, 0.55.

The upswings in beating frequency upon addition of ATP were also comparable between the mutant and WT (Fig. 3C). Moreover, a defect in ciliary motility is thought to underlie the randomization of left-right asymmetry by abolishing a leftward flow of extraembryonic fluid during early development (15). No defects in left-right body axis determination were found in the homozygous mice. The sensory cilia may also move at a much lower rate. Photoreceptor inner and outer segments are aligned along different axes (10). Cells at the posterior retina are vertically aligned, but those at the peripheral retina have outer and inner segments at an angle to each other, presumably for the purpose of optical alignment (Stiles-Crawford effect) (20). An active movement mechanism is thought to maintain this alignment (2). Examination of retinal sections showed that the alignments of inner and outer segments were similar between the mutant and controls. These observations suggest that the ciliary rootlet is not fundamental to ciliary motility.

Protein trafficking between the inner and outer segments of photoreceptors is highly active. The facts that rootlets span the entire length of the photoreceptor cell bodies, that rootletin interacts with the kinesin light chain (26), and that a previous study implicated rootlets as a route for the transport of the peripherin/RDS protein (4) prompted us to examine a putative role for the rootlet in protein trafficking. A hypothesis was that the rootlet might help organize a track system along which movements of molecular motors take place. If it did play such

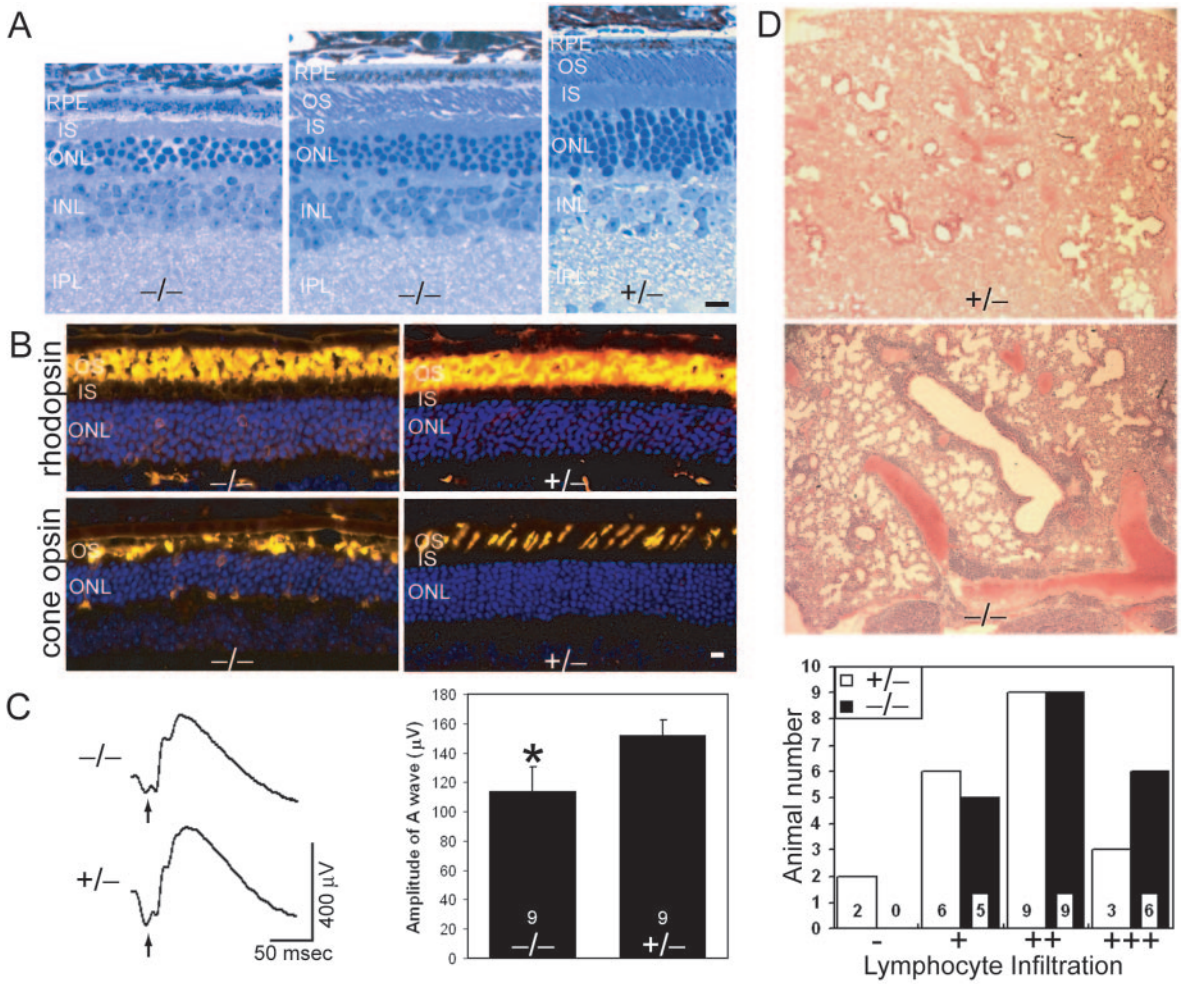

FIG. 4. Retinal degeneration and lung lymphocyte infiltration in the rootletin mutant. (A) Defective outer segments and reduced nuclear layer thickness were seen at 18 months of age in mutant (–/–) retinas. There was variability in the extent of photoreceptor degeneration within the retina, with severely affected areas having no outer segments remaining (left panel) and better-preserved areas having shortened and disorganized outer segments (middle panel). (Right panel) Age-matched control. (B) Immunofluorescence shows mislocalization of rhodopsin and cone opsin in mutant photoreceptors. Nuclei (blue) were counterstained blue with Hoechst dye. (C) ERGs show reduced a-wave (arrows) amplitudes in the mutant (–/–). (Left) Representative ERG tracings. (Right) Bar graphs comparing ERG a-wave amplitudes (means ± standard errors of the means [SEM]; nine mice were used for each genotype; $P < 0.05$) of the mutant (–/–) and control (+/–). (D) Increased lymphocyte infiltration in the mutant lung. (Upper panels) Hematoxylin- and eosin-stained lung sections showing an increase in lymphocyte infiltration in the mutant lungs (blue nuclear stain). A control lung graded "–" and a mutant lung graded "+++" are shown. (Lower panel) Bar graph showing the grade (as defined in Materials and Methods) distribution among mutant and control lungs. RPE, retinal pigment epithelium; OS, outer segment; IS, inner segment; ONL, outer (photoreceptor) nuclear layer; INL, inner nuclear layer; IPL, inner plexiform layer. Bars, 10 μm.

a role and if this role was nonredundant, then the highly specific localization patterns of the outer segment proteins would not be maintained. To investigate this issue, we examined the subcellular localization of rhodopsin, cone opsin, and peripherin/RDS in rootlet-null photoreceptor cells. They were found to have a normal distribution (data not shown). Transducin and arrestin undergo rapid light-driven movement in normal photoreceptors (18, 23). This movement was found to also occur in the rootletin mutant photoreceptors (data not shown). Finally, a defect in protein trafficking may lead to shorter outer segments by retarding their initial development or subsequent renewal. We found normal lengths of photoreceptor outer segments on postnatal day 20, when photoreceptors are still developing, and on day 60, when photoreceptors are fully mature (data not shown). Thus, any participation of the ciliary rootlets in trafficking pathways must be at least partially redundant and was not detected by our assays in this study.

The rootlet is required for long-term maintenance of ciliated cells. Although the "rootletless" photoreceptors initially had normal histology and function, their life span was reduced. At 18 months, mutant retinas showed clear signs of photoreceptor degeneration. These include shortening, disorganization, and loss of the outer segments, reduced thickness of the cell nuclear layer (Fig. 4A), and mislocalization of rod and cone opsins (Fig. 4B). ERG measurements of 18-month-old mutant mice found a significant reduction in the a-wave amplitude (Fig. 4C), which could be attributed to the outer segment

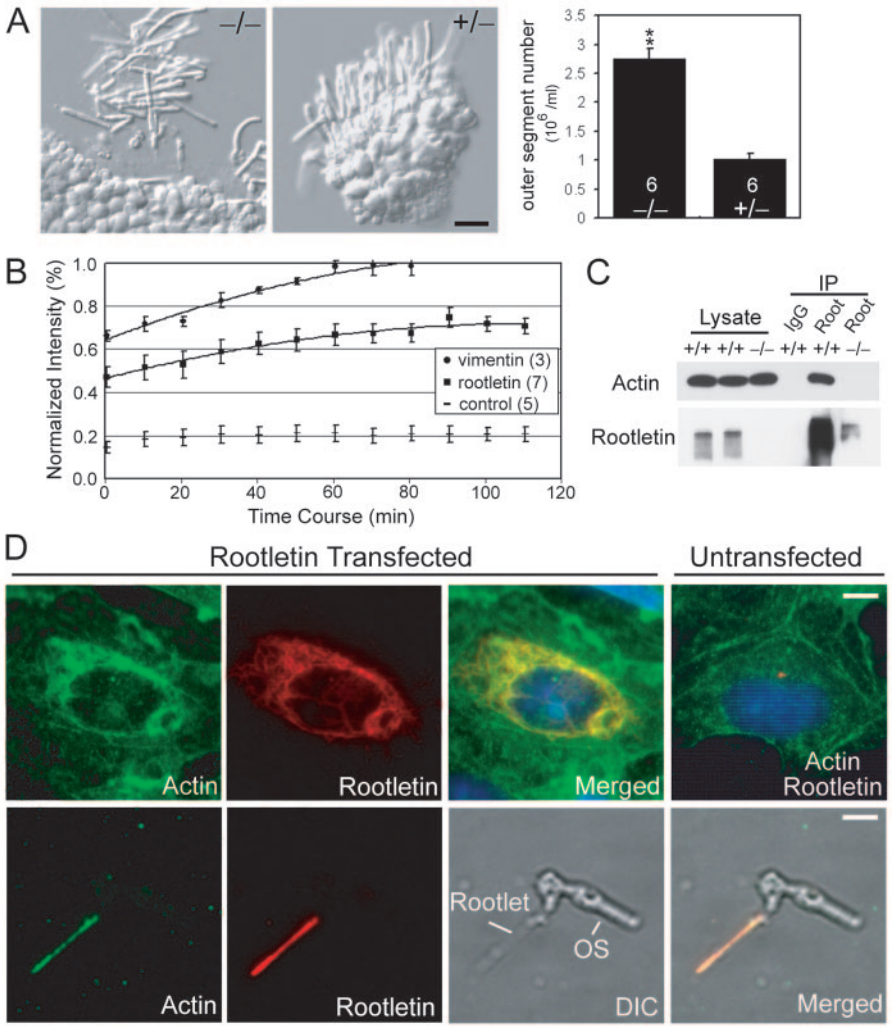

FIG. 5. The ciliary rootlet as an essential support structure for the cilium. (A) Fragility of photoreceptors lacking rootlets. (Left) Nomarski images of dissected retinas indicating mutant photoreceptors are much more prone to breakage at the ciliary base. Bar, 10 μm. (Right) Quantification of the data shown in a bar graph (mean ± SEM, $n = 6$ for each genotype, $P < 0.01$). (B) Static nature of rootletin fibers shown by quantitative FRAP analysis. The numbers in the parentheses are sample numbers. (C) Interaction of rootletin with actin shown by coimmunoprecipitation. IgG, normal rabbit immunoglobulin G; Root, rabbit antirootletin antibody; IP, immunoprecipitate; Input (cell lysate), 5%. (D) Colocalization of rootletin and actin filaments by immunofluorescence. (Upper panel) Recombinant rootletin polymers cause a redistribution of actin filaments so that a fraction of the actin filaments colocalizes with the rootlet fibers. (Lower panel) Actin colocalizes with the native rootlet in a photoreceptor cell. OS, outer segment; DIC, differential-interference contrast. Bars, 5 μm.

defect and photoreceptor cell loss. Thus, ciliary rootlets are essential for the long-term survival of the photoreceptors.

To ascertain if the rootlet is dispensable for motile cilia, we examined lungs in the aged mutant mice for evidence for chronic obstructive pulmonary disease. This could arise if mucociliary clearance was compromised as a result of motile cilium defects. We found no significant alveolar wall destruction, subepithelial fibrosis in the bronchioles, or accumulation of Charcot-Leyden crystal-like deposits, which are hallmarks of allergic inflammation. We did see an increased incidence of lymphocyte infiltration around bronchioles and blood vessels in the mutant lungs (Fig. 4D). Lymphocyte infiltration occurred in mice of advanced age (18 to 24 months), which approaches the natural life span of the mice, suggesting that the deleterious effect is subtle and takes considerable time to become manifest. These findings do suggest that loss of the rootlets has a negative impact on motile cilium function and/or maintenance.

The ciliary rootlet provides essential structural support. We postulated that the photoreceptor cell death and pathological changes in the lung in the mutant might arise from a compromise in structural integrity of ciliated cells. We noticed that under conditions of gentle dissection, the inner segments of mutant photoreceptor cells easily broke apart, while the control photoreceptor cells remained intact (Fig. 5A). To quantify the fragility of photoreceptor cells, we counted the number of the broken outer segments in the same volume of media in which the retina was dissected. The number of broken outer segments from the mutant retina was about 2.7-fold higher than the ones from the control retina (Fig. 5A). The Student *t*

test showed a significant difference between the two groups ($P < 0.01$). Thus, this result suggests that the rootlet-null photoreceptors may also be vulnerable to the mechanical stress in vivo. Our finding of a much higher percentage of nonresponsive cells during single-cell recording, which involved gentle dissection, was consistent with this interpretation.

Furthermore, we reasoned that if the ciliary rootlet provides critical structural support, it should have a static and stable structure. We studied the dynamics of monomer-polymer exchange in the recombinant rootletin fibers in COS cells. Time-lapse fluorescence recording found little active growth and shortening of the individual green fluorescent protein-tagged rootletin fibers in the span of 20 min (data not shown), suggesting that the rootletin fibers are not under constant flux at their ends. To study the dynamics of the recombinant rootletin along its fibers, we performed FRAP, a technique that has been widely used to study cytoskeleton dynamics. In this assay, the time required for fluorescence recovery in the bleached region of a polymer gives a measure of the exchange rate between the polymer and monomers in the cytoplasm. As shown in Fig. 5B, it took 110 min for rootletin fibers to recover about 70% of its original fluorescence. At this time point the recovery phase appeared to have reached a plateau, suggesting that the remaining 30% of rootletin polymer would take much longer to undergo complete exchange, if it occurred at all. In comparison, green fluorescent protein-tagged vimentin, an intermediate filament protein known to be less dynamic than microtubules and actin filaments, took a shorter time to fully recover. Thus, the rootletin fibers appear even more stable than vimentin. In addition, during the FRAP experiment of rootletin, we did not detect any polarity of the fluorescence recovery along the bleached rootletin fibers or any migration of the bleached regions towards either the centrosome or the cell periphery, indicating no polarization of rootletin polymerization and no treadmilling for rootletin fibers.

For the ciliary rootlet to function as a strong structural support, it was expected to integrate with other cytoskeletal systems within the cell. We therefore investigated whether there are physical interactions between the rootlet and actin filaments or microtubules. We performed immunoprecipitation of rootletin from control and mutant retinal lysates and found that actin, but not tubulin, coprecipitated with rootletin (Fig. 5C). Actin was also coimmunoprecipitated with recombinant rootletin from COS cell lysate (data not shown). We then asked if there was colocalization between the rootlets and actin filaments. In COS cells transfected with rootletin, there was varied overlap between rootletin and actin immunostaining signals, some with substantial overlap (Fig. 5D, upper panels). In comparison, there was little overlap between rootletin fibers and microtubules (data not shown). To validate these findings in vivo, we performed double labeling for actin and rootletin in photoreceptor cells and found strong actin staining along the rootlet (Fig. 5D, lower panels). These results suggest that the ciliary rootlets stably associate with actin filaments in ciliated cells.

The ciliary rootlet is involved in organizing cellular organelles. Large membranous saccules normally wrap around the rootlets through the length of the photoreceptor inner segments, which are visible by electron microscopy on both longitudinal (26) and cross (Fig. 6A) sections. By electron microscopy, we found that, in the absence of the rootlets, these membranous organelles became randomized in the inner segments (Fig. 6A and B). Changes in the orientation of the basal bodies were also notable; on average, basal bodies in mutant photoreceptors are arranged at much larger angles than they are in the WT (Fig. 2D and 6C). Localization of the mitochondria, normally concentrated around the periphery of apical inner segments, remained unchanged in the mutant (Fig. 6A).

DISCUSSION

This study has resolved the long-standing question concerning the structure and function of the striated ciliary rootlet. To study the in vivo functions of the ciliary rootlet, we created and analyzed lines of rootletin mutant mice. Elimination of rootletin expression ablated ciliary rootlets in all ciliated cells. This finding formally demonstrates that rootletin is the major, and likely only, structural component of the ciliary rootlet. Our analyses of the mutant mice devoid of rootlets help define the in vivo functions of this structure. Thus, the rootlets were found to be dispensable for ciliary development and basal functions but required for the long-term stability of some types of cilia. Among them, the photoreceptors stand out as the type of cells particularly sensitive to a loss of the rootlets. This is almost certainly due to the fact that photoreceptors elaborate the light-sensing outer segments, the largest mammalian cilia by far. Any shear force encountered by the outer segments would be magnified multiple times by the leverage effect when sensed at the point of anchor. Within the connecting cilia and basal outer segments, the tightly packed axonemal microtubule bundles provide rigidity and support. At points proximal to the basal bodies, it appears that the ciliary rootlet assumes a major structural role. Indeed, gentle dissection of the retina in vitro causes massive breakage of the "rootletless" photoreceptors, primarily at the junction between inner and outer segments and sometimes within the inner segments. The age-dependent photoreceptor degeneration in the mutant mice may therefore be attributed, at least in part, to an increased vulnerability to mechanical stress.

The in vitro experiments in the present study lend support to the notion that the rootlets function primarily as a support structure. First, we demonstrate by time-lapse fluorescence recording and FRAP experiments that the rootletin fibrous network in transfected cells is a very stable structure. These findings are consistent with our previous report that recombinant rootletin fibers do not fully disassemble even during mitosis, suggesting that rootletin fibers are among the least dynamic of all cytoskeletons. There are three major fibrous cytoskeletal networks in cells: microtubules, actin filaments, and intermediate filaments. The first two are usually more dynamic, undergoing active changes in their lengths and rapid recovery in FRAP experiments (1, 16). Intermediate filaments are relatively more stable (8, 21, 27, 28). Rootletin shares certain structural characteristics with intermediate filaments. Both rely on rod domains for polymerization and lateral interactions. Indeed, the recovery time for rootletin in FRAP experiments is similar to that of keratin, the most stable form of intermediate filaments. Mutations or deletions of keratins cause blistering skin diseases (6), indicating that keratins confer critical structural stability to epidermis against mechanical

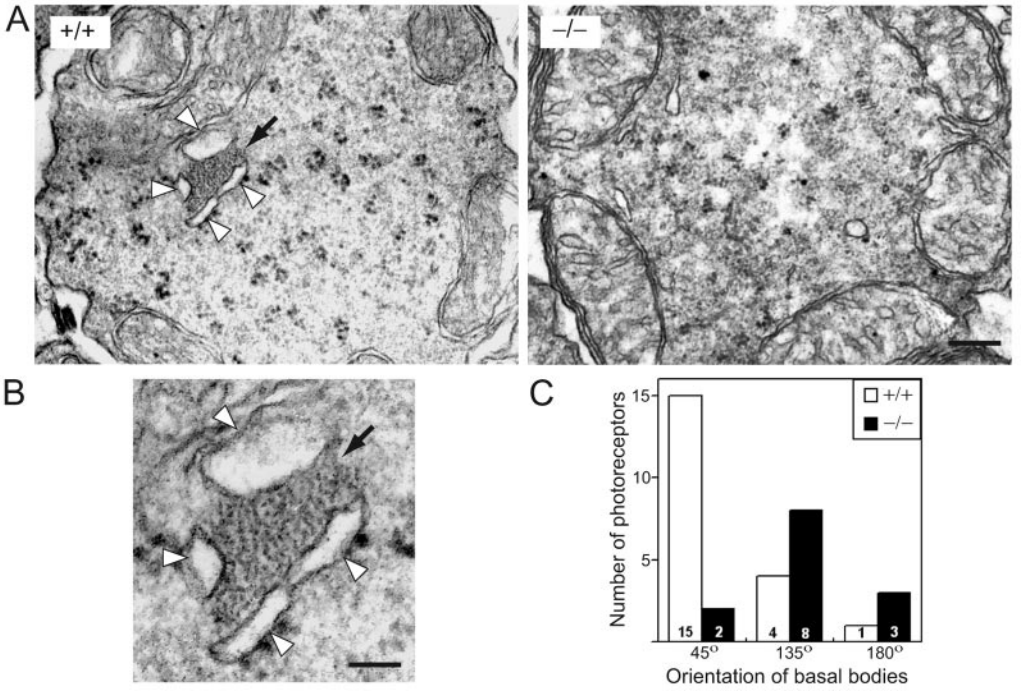

FIG. 6. The rootlet is an organizer for cellular organelles in photoreceptors. (A) Cross sections through the apical region of photoreceptor inner segments show membranous saccules surrounding the rootlet fibers (arrow) in the WT (+/+) but randomized saccules in the mutant (–/–). The localization of mitochondria, normally concentrated around the periphery of a cell, remains unchanged in the mutant. Bar, 0.15 μm. (B) Higher-magnification image from the WT in panel A, focusing on the rootlet and surrounding membranes. Bar, 60 nm. (C) Bar graph showing the counts of basal body pairs arranged in different angular relationships.

stress. Thus, the similarity in structure and dynamics that rootletin shares with intermediate filaments supports the in vivo function of the ciliary rootlet in mechanical support.

Second, we present evidence that the ciliary rootlet integrates with actin filaments, which are known to support cells against mechanical stress. In photoreceptor cells, actin filaments exist throughout the cells. They are especially enriched in the distal end of the inner segments, where the rootlets originate. Thus, the integration between these two cytoskeletal networks in cells probably enhances the structural support of the ciliary rootlet. Because we did not find actin as a rootletin-interacting protein in our previous yeast two-hybrid screen using the rootletin fragments as baits, the integration between rootletin and actin may be indirect, or the interaction occurs only between filamentous forms of the two cytoskeletal proteins. The association between rootletin and actin filaments and a reported interaction between the rootlet and intermediate filaments (11) may contribute substantially to the role of the rootlet as an important support structure.

The present study confirms that rootlets serve to anchor membranous organelles within the photoreceptor inner segments. Large membranous saccules that normally surround the rootlets in photoreceptor inner segments become randomized in the absence of rootlets. It is possible, though unconfirmed, that an interaction between rootletin and the cortical actin filaments on the cytoplasmic faces of the membranes is responsible for the congregation of membranes around the rootlets. Also unclear at the present is the identity of the membranous saccules and how much, if any, the loss of anchor to these membranous organelles contributes to the photoreceptor degeneration.

The present study also identifies rootletin as a candidate gene for human retinal degeneration. Based on the murine data, the corresponding human retinal degeneration may be one of late onset, possibly with systemic manifestation of a ciliary defect, such as respiratory tract symptoms. The disease course of rootletin-related retinal degeneration may be influenced by cumulative life experiences. For example, sport or job-related activities that are prone to high levels of physical impact might well exacerbate the course of disease. From this perspective, identification of rootletin gene mutations that cause retinal degeneration may provide both prognostic and treatment benefits to patients.

ACKNOWLEDGMENTS

We thank Guohua Yue for help in constructing the targeting vector; Norman Michaud and Akella Sreedevi for some histology preparations; O. Bulgakov, D. Hong, E. Mark, M. Sandberg, X. Liu, and Y. Zhao for suggestions; and Shioko Kimura for the Ym1 antibody.

This work was supported by grants from the National Institutes of Health (EY16442, EY11358, EY14104, and EY12950), Philip Morris USA Inc. and Philip Morris International, and the Foundation Fighting Blindness.

REFERENCES

1. **Amato, P. A., and D. L. Taylor.** 1986. Probing the mechanism of incorporation of fluorescently labeled actin into stress fibers. J. Cell Biol. **102:**1074–1084.
2. **Applegate, R. A., and A. B. Bonds.** 1981. Induced movement of receptor alignment toward a new pupillary aperture. Investig. Ophthalmol. Vis. Sci. **21:**869–872.

3. **Besharse, J. C., and C. J. Horst.** 1990. The photoreceptor connecting cilium: a model for the transition zone, p. 389–417. *In* R. A. Bloodgood (ed.), Ciliary and flagellar membranes. Plenum, New York, N.Y.
4. **Fariss, R. N., R. S. Molday, S. K. Fisher, and B. Matsumoto.** 1997. Evidence from normal and degenerating photoreceptors that two outer segment integral membrane proteins have separate transport pathways. J. Comp. Neurol. **387:**148–156.
5. **Fawcett, D. W., and K. R. Porter.** 1954. A study of the fine structure of ciliated epithelia. J. Morphol. **94:**221–282.
6. **Fuchs, E.** 1995. Keratins and the skin. Annu. Rev. Cell Dev. Biol. **11:**123–153.
7. **Guo, L., R. S. Johnson, and J. C. Schuh.** 2000. Biochemical characterization of endogenously formed eosinophilic crystals in the lungs of mice. J. Biol. Chem. **275:**8032–8037.
8. **Ho, C. L., J. L. Martys, A. Mikhailov, G. G. Gundersen, and R. K. Liem.** 1998. Novel features of intermediate filament dynamics revealed by green fluorescent protein chimeras. J. Cell Sci. **111:**1767–1778.
9. **Hong, D. H., B. Pawlyk, M. Sokolov, K. J. Strissel, J. Yang, B. Tulloch, A. F. Wright, V. Y. Arshavsky, and T. Li.** 2003. RPGR isoforms in photoreceptor connecting cilia and the transitional zone of motile cilia. Investig. Ophthalmol. Vis. Sci. **44:**2413–2421.
10. **Laties, A. M., and J. M. Enoch.** 1971. An analysis of retinal receptor orientation. I. Angular relationship of neighboring photoreceptors. Investig. Ophthalmol. **10:**69–77.
11. **Lemullois, M., P. Gounon, and D. Sandoz.** 1987. Relationships between cytokeratin filaments and centriolar derivatives during ciliogenesis in the quail oviduct. Biol. Cell **61:**39–49.
12. **Li, T., M. A. Sandberg, B. S. Pawlyk, B. Rosner, K. C. Hayes, T. P. Dryja, and E. L. Berson.** 1998. Effect of vitamin A supplementation on rhodopsin mutants threonine-17→methionine and proline-347→serine in transgenic mice and in cell cultures. Proc. Natl. Acad. Sci. USA **95:**11933–11938.
13. **Liu, X., O. V. Bulgakov, X. H. Wen, M. L. Woodruff, B. Pawlyk, J. Yang, G. L. Fain, M. A. Sandberg, C. L. Makino, and T. Li.** 2004. AIPL1, the protein that is defective in Leber congenital amaurosis, is essential for the biosynthesis of retinal rod cGMP phosphodiesterase. Proc. Natl. Acad. Sci. USA **101:**13903–13908.
14. **Molday, R.** 1988. Monoclonal antibodies to rhodopsin and other proteins of rod outer segments. Prog. Retin. Eye Res. **8:**173–209.
15. **Nonaka, S., Y. Tanaka, Y. Okada, S. Takeda, A. Harada, Y. Kanai, M. Kido, and N. Hirokawa.** 1998. Randomization of left-right asymmetry due to loss of nodal cilia generating leftward flow of extraembryonic fluid in mice lacking KIF3B motor protein. Cell **95:**829–837.
16. **Saxton, W. M., D. L. Stemple, R. J. Leslie, E. D. Salmon, M. Zavortink, and J. R. McIntosh.** 1984. Tubulin dynamics in cultured mammalian cells. J. Cell Biol. **99:**2175–2186.
17. **Sjostrand, F. S.** 1953. The ultrastructure of the inner segments of the retinal rods of the guinea pig eye as revealed by electron microscopy. J. Cell. Comp. Physiol. **42:**45–70.
18. **Sokolov, M., A. L. Lyubarsky, K. J. Strissel, A. B. Savchenko, V. I. Govardovskii, E. N. Pugh, Jr., and V. Y. Arshavsky.** 2002. Massive light-driven translocation of transducin between the two major compartments of rod cells: a novel mechanism of light adaptation. Neuron **34:**95–106.
19. **Spira, A. W., and G. E. Milman.** 1979. The structure and distribution of the cross-striated fibril and associated membranes in guinea pig photoreceptors. Am. J. Anat. **155:**319–337.
20. **Stiles, W. S., and B. H. Crawford.** 1933. The luminous efficiency of rays entering the eye pupil at different points. Proc. R. Soc. London **112:**428–450.
21. **Vikstrom, K. L., S. S. Lim, R. D. Goldman, and G. G. Borisy.** 1992. Steady state dynamics of intermediate filament networks. J. Cell Biol. **118:**121–129.
22. **Ward, J. M., M. Yoon, M. R. Anver, D. C. Haines, G. Kudo, F. J. Gonzalez, and S. Kimura.** 2001. Hyalinosis and Ym1/Ym2 gene expression in the stomach and respiratory tract of 129S4/SvJae and wild-type and CYP1A2-null B6, 129 mice. Am. J. Pathol. **158:**323–332.
23. **Whelan, J. P., and J. F. McGinnis.** 1988. Light-dependent subcellular movement of photoreceptor proteins. J. Neurosci. Res. **20:**263–270.
24. **Wolfrum, U.** 1992. Cytoskeletal elements in arthropod sensilla and mammalian photoreceptors. Biol. Cell **76:**373–381.
25. **Worley, L. G., E. Fischbein, and J. E. Shapiro.** 1953. The structure of ciliated epithelial cells as revealed by the electron microscope and in phase contrast. J. Morphol. **92:**545–577.
26. **Yang, J., X. Liu, G. Yue, M. Adamian, O. Bulgakov, and T. Li.** 2002. Rootletin, a novel coiled-coil protein, is a structural component of the ciliary rootlet. J. Cell Biol. **159:**431–440.
27. **Yoon, K. H., M. Yoon, R. D. Moir, S. Khuon, F. W. Flitney, and R. D. Goldman.** 2001. Insights into the dynamic properties of keratin intermediate filaments in living epithelial cells. J. Cell Biol. **153:**503–516.
28. **Yoon, M., R. D. Moir, V. Prahlad, and R. D. Goldman.** 1998. Motile properties of vimentin intermediate filament networks in living cells. J. Cell Biol. **143:**147–157.
29. **Zhang, L., and M. J. Sanderson.** 2003. Oscillations in ciliary beat frequency and intracellular calcium concentration in rabbit tracheal epithelial cells induced by ATP. J. Physiol. **546:**733–749.